



Catalytic activation and reforming of methane on supported palladium clusters

Aritomo Yamaguchi, Enrique Iglesia*

Department of Chemical Engineering, University of California at Berkeley, Berkeley, CA 94720, United States

ARTICLE INFO

Article history:

Received 29 March 2010

Revised 25 May 2010

Accepted 2 June 2010

Available online 8 July 2010

Keywords:

Methane reforming

Palladium catalysts

C–H bond activation

Elementary steps for CH₄ reactions

Isotopic tracer

ABSTRACT

The effects of reactant and product concentrations on turnover rates and isotopic tracing and kinetic isotope effects have led to a sequence of elementary steps for CH₄ reactions with CO₂ and H₂O on supported Pd catalysts. Rate constants for kinetically-relevant C–H bond activation steps are much larger on Pd than on other metals (Ni, Ru, Rh, Ir, Pt). As a result, these steps become reversible during catalysis, because the products of CH₄ dissociation rapidly deplete the required oxygen co-reactant formed from CO₂ or H₂O and co-reactant activation, and water–gas shift reactions remain irreversible in the time scale required for CH₄ conversion. H₂ and CO products inhibit CH₄ reactions via their respective effects on CH₄ and CO dissociation steps. These mechanistic conclusions are consistent with the kinetic effects of reactants and products on turnover rates, with the similar and normal CH₄/CD₄ kinetic isotope effects measured with H₂O and CO₂ co-reactants, with the absence of H₂O/D₂O isotope effects, and with the rate of isotopic scrambling between CH₄ and CD₄, ¹²C¹⁶O and ¹³C¹⁸O, and ¹³CO and ¹²CO during CH₄ reforming catalysis. This catalytic sequence, but not the reversibility of its elementary steps, is identical to that reported on other Group VIII metals. Turnover rates are similar on Pd clusters on various supports (Al₂O₃, ZrO₂, ZrO₂–La₂O₃) and independent of Pd dispersion over the narrow range accessible at reforming conditions, because kinetically-relevant C–H bond activation steps occur predominantly on Pd surfaces. ZrO₂ and ZrO₂–La₂O₃ supports, with detectable reactivity for CO₂ and H₂O activation, can reverse the infrequent formation of carbon overlayers and inhibit deactivation, but do not contribute to steady-state catalytic reforming rates. The high reactivity of Pd surfaces in C–H bond activation reflects their strong binding for C and H and the concomitant stabilization of the transition state for kinetically-relevant C–H activation steps and causes the observed kinetic inhibition by chemisorbed carbon species formed in CH₄ and CO dissociation steps.

© 2010 Elsevier Inc. All rights reserved.

1. Introduction

CH₄ activation and reforming reactions using CO₂ or H₂O co-reactants provide attractive routes to synthesis gas (H₂/CO) or H₂ streams [1,2] and to carbon nanostructures [3] from natural gas. Group VIII metals catalyze CH₄ reforming and decomposition [1,2], but strong C–H bonds (439 kJ mol⁻¹ [4]) lead to endothermic processes that require high temperatures for practical CH₄ conversions and, as a result, also catalytic materials that resist sintering and carbon formation at severe operating conditions. The detailed sequence of elementary steps and their kinetic relevance, as well the effects of metal cluster size and supports, remain controversial, at least in part because of ubiquitous thermodynamic and transport corruptions of reaction rates, often measured at conditions near thermodynamic equilibrium.

Our previous studies have addressed these mechanistic and practical matters for CH₄ reforming with CO₂ and H₂O co-reactants and for CH₄ decomposition on supported Ni, Ru, Rh, Pt, and Ir clus-

ters [5,6]. Reaction rates, after being corrected for approach to equilibrium, depend linearly on CH₄ pressure but are insensitive to the identity or concentration of the co-reactants on all these catalysts. Measured turnover rates, isotopic tracing, and kinetic isotope effects, obtained under conditions of strict kinetic control, showed that C–H bond activation is the sole kinetically-relevant step and that neither reactants nor products lead to significant surface coverages of reactive intermediates during steady-state catalysis. On all metals, turnover rates for H₂O and CO₂ reforming increased as clusters became smaller, because coordinatively unsaturated surface atoms, prevalent on small clusters, tend to stabilize C and H atoms and the transition states involved in C–H bond activation more effectively than more highly coordinated surface atoms on low-index surfaces. The extreme unsaturation of surface atoms at corners or edges may lead, however, to unreactive carbon, rendering such sites permanently unavailable at all reforming reaction conditions. Supports did not influence C–H activation turnover rates, except through their effect on metal dispersion, as expected from the sole kinetic relevance of C–H bond activation steps and from their exclusive occurrence on metal clusters. Co-reactant activation steps and all elementary steps involved in

* Corresponding author. Fax: +1 510 642 4778.

E-mail address: iglesia@berkeley.edu (E. Iglesia).

water–gas shift reactions remained quasi-equilibrated on these metals at all reaction conditions examined, consistent with isotopic tracer data that showed carbon, oxygen, and hydrogen isotopic equilibration for CO–CO₂ and H₂O–H₂ during CH₄ reforming catalysis.

We provide evidence here for a similar sequence of elementary steps on Pd clusters. Pd atoms at clusters surfaces are much more reactive for C–H bond activation than on surfaces of the other Group VIII metals. These fast reactions scavenge active O* species from co-reactants and prevent the equilibration of co-reactant activation steps and of water–gas shift on Pd metal surfaces, in contrast with the equilibrated nature of these steps on less reactive metals. In addition, the kinetic coupling of fast C–H activation steps on Pd with the steps that form O* causes inhibition effects by products, as a result of the reversibility of both C–H and C–O activation steps.

Sintering and carbon formation have impaired previous attempts at kinetic measurements and at their rigorous mechanistic interpretations for CH₄ reforming on Pd catalysts [7–10]. Supports and additives (e.g., La, Ce oxides) have been used to inhibit carbon formation [8,11], apparently because they can activate CO₂ at conditions (low CO₂/CH₄ ratios) that prevent the effective removal of chemisorbed carbon via reactions with CO₂-derived O* on monofunctional catalysts, except through the assistance of co-reactant activation on supports. These support effects have been claimed as evidence for the kinetic relevance of CO₂ dissociation [7]. Yet other studies conclude that only C–H bond activation steps control the rates of CH₄ reforming on Group VIII metals [2], consistent with the normal kinetic isotopic effects ($r_{\text{CH}_4}/r_{\text{CD}_4}$) observed on most metal surfaces and with their similar values and rate equations with H₂O and CO₂ co-reactants [5,6,12].

Here, we probe the elementary steps involved in CH₄ reactions on Pd-based catalysts and provide evidence for a sequence of elementary steps consistent with rate and isotopic data obtained under conditions of strict kinetic control. These data show that C–H bond activation steps on Pd are kinetically-relevant but reversible, even at conditions for which the overall reforming reaction is essentially irreversible, in contrast with their irreversible nature on other Group VIII metals [5,6]. Pd clusters provide the most active surfaces for C–H bond activation among Group VIII metals, but the kinetic coupling of these steps with co-reactant activation steps leads to inhibition by the H₂ and CO products of reforming reactions. Supports do contribute to steady-state turnover rates, but their ability to activate co-reactants can be used to reverse the occasional blockage of Pd cluster surfaces during steady-state CH₄ reforming.

2. Experimental methods

2.1. Catalysts synthesis and characterization

ZrO₂ and γ -Al₂O₃ were prepared as described previously [6]. ZrO₂ was prepared by hydrolysis of an aqueous solution of ZrCl₂·8H₂O (Aldrich, >98% wt.) at a constant pH of 10 and subsequent filtration, drying, and treatment in flowing dry air (Praxair, UHP, 1.2 cm³ g⁻¹ s⁻¹) at 923 K (0.167 K s⁻¹) for 5 h. γ -Al₂O₃ was prepared by treating Al(OH)₃ (Aldrich) in flowing dry air (Praxair, UHP, 1.2 cm³ g⁻¹ s⁻¹) at 923 K (0.167 K s⁻¹) for 5 h. Pd/ZrO₂ and Pd/Al₂O₃ samples were prepared by incipient wetness impregnation of ZrO₂ or γ -Al₂O₃ with an aqueous solution of Pd(NO₃)₂ (Alfa Aesar, 99.9%) and treatment in ambient air at 393 K. These samples were treated in flowing dry air (Praxair, UHP, 1.2 cm³ g⁻¹ s⁻¹) at 923 K (heating rate 0.167 K s⁻¹) for 5 h and then in flowing H₂ (Praxair, UHP, 50 cm³ g⁻¹ s⁻¹) at 1023 K (heating rate 0.167 K s⁻¹) for 2 h. Pd/ZrO₂-La₂O₃ was prepared by incipient wetness impregnation of Pd/ZrO₂ (treated in H₂ as described above) with an aqueous solution of La(NO₃)₃·6H₂O (Aldrich, 99.999%), treatment in

flowing dry air (Praxair, UHP, 1.2 cm³ g⁻¹ s⁻¹) at 923 K (0.167 K s⁻¹) for 3 h and then in H₂ (Praxair, UHP, 50 cm³ g⁻¹ s⁻¹) at each temperature for 2 h.

The dispersion of Pd clusters, defined as the ratio of all Pd atoms exposed at surfaces, was measured by O₂ adsorption and titration of adsorbed oxygen by H₂ at 373 K in a volumetric unit (Quantachrome, Autosorb-1). Samples were treated in H₂ (Praxair, UHP) at 653 K (0.167 K s⁻¹) for 1 h and evacuated at 653 K for 1 h to remove chemisorbed hydrogen. Saturation monolayer uptakes were estimated by extrapolating isotherms to zero pressure. The number of exposed Pd metal atom was estimated by assuming one chemisorbed oxygen atom per exposed Pd atom [13].

2.2. Methane reaction rate and isotopic measurements

Rates were measured in a packed-bed reactor with plug-flow hydrodynamics. Pd catalysts (5 mg) were diluted with 25 mg of γ -Al₂O₃ within catalyst pellets (250–425 μ m pellet diameter) and then physically mixed with acid-washed quartz (500 mg, 250–425 μ m). These samples were placed in a quartz tube (8 mm diameter) with a K-type thermocouple enclosed within a quartz sheath in contact with the catalyst bed. Reactants consisted of mixtures of 50% CH₄/Ar (Praxair, Certified standard), 50% CO₂/N₂ (Praxair, Certified standard), and He (Praxair, UHP) metered by electronic flow controllers. H₂O (deionized water) was introduced using a syringe pump (Cole-Parmer, 74900 series) into the reactant stream by vaporizing into a stainless line kept at 423 K. All transfer lines from the injection point to the gas chromatograph were kept above 410 K to avoid condensation. The concentrations of reactants and products were measured by on-line gas chromatography (Agilent, 6890 series) using a HayeSep A (3.2 mm \times 10 m) column and a thermal conductivity detector.

Kinetic isotopic effects were measured for CH₄ reforming on a 1.6% wt. Pd/ZrO₂ catalyst using the same reactor system using CH₄-CO₂ and CD₄-CO₂ reactants for CO₂ reforming and CH₄-H₂O, CD₄-H₂O, and CD₄-D₂O reactants for H₂O reforming. CD₄ (Isotec, 99 atom % deuterium) and D₂O (Isotec, 99.9 atom % deuterium) were used as reactants without further purification. Isotopic exchange data were also measured on this catalyst using on-line mass spectrometry (Inficon, Transpector series). The reactants consisted of 50% CH₄/Ar (Praxair, Certified standard), 50% CO₂/He (Praxair, Certified standard), Ar (Praxair, UHP), and He (Praxair, UHP) all metered using electronic flow controllers. CD₄ (Isotec, 99 atom % deuterium), D₂ (Matheson, 99.7%), ¹³C (Isotec, 99 atom % ¹³C), and ¹³C¹⁸O (Isotec-Sigma-Aldrich, 99 atom % ¹³C, 95 atom % ¹⁸O) were used as reactants without further purification. Concentrations of CH₄, CO, CO₂ isotopomers were estimated from mass spectra using matrix deconvolution methods [14].

3. Results and discussion

3.1. Catalyst characterization

All catalysts used in this study are listed in Table 1. These samples were treated in H₂ at temperatures higher than those used in CH₄ reforming reactions to prevent further structural changes during catalysis. The mean cluster size in each sample was estimated from Pd dispersions measured from chemisorption uptakes by assuming hemispherical crystallites and the atomic density of bulk Pd. The Pd cluster diameter for the 1.6% wt. Pd/ZrO₂ sample treated in H₂ at 1023 K (denoted hereinafter as 1.6% wt. Pd/ZrO₂(1023)) was 12.5 nm. The Pd cluster size increased with increasing H₂ treatment temperature and reached a value of 32 nm after H₂ treatment at 1123 K (1.6% wt. Pd/ZrO₂(1123)), a value consistent with the Pd cluster size derived from transmission electron microscopy (31 nm mean cluster diameter, Fig. S1).

Table 1
Reduction temperature, Pd dispersion, and mean particle size of supported Pd catalysts.

Catalyst	Reduction temperature (K)	Dispersion (%) ^a	Mean particle size (nm) ^b
1.6% wt. Pd/ZrO ₂	1023	8.9	12.5
1.6% wt. Pd/ZrO ₂ –La ₂ O ₃	1023	5.3	21.1
1.6% wt. Pd/Al ₂ O ₃	1023	7.5	14.9
1.6% wt. Pd/ZrO ₂	1123	3.5	32.0

^a The fraction of the surface Pd atoms from O₂ chemisorption and titration of chemisorbed oxygen by H₂.

^b The mean particle size (*D*) was estimated from Pd dispersion (*d*) using $D = 1.1/d$.

CH₄–CO₂ turnover rates were measured on Pd/ZrO₂(1023), Pd/ZrO₂–La₂O₃(1023), and Pd/Al₂O₃(1023) (1.6% wt.; Fig. 1). CH₄ turnover rates were stable with time on Pd/ZrO₂ and Pd/ZrO₂–La₂O₃; Pd/Al₂O₃ deactivated during reaction, indicating that ZrO₂ and ZrO₂–La₂O₃ supports stabilize Pd clusters against deactivation. Pd clusters on Al₂O₃ appeared to grow or become covered with unreactive species during CH₄ reforming [15]. Initial CH₄ turnover rates were similar on Pd clusters dispersed on all three supports. The low and similar dispersion (5.3–8.9%, Table 1) of these samples causes reactions to occur predominantly at low-index planes, which prevail on large clusters. The fraction of surface atoms exposed at edges and corners decreases monotonically with increasing cluster size [16], but their high reactivity tends to be dampened by their tendency to form strongly-bound CH₄-derived species [17,18] that are removed too slowly for significant contributions to reforming turnovers.

We conclude from these data that these supports do not influence turnover rates on Pd clusters because of their low reactivity in activation of H₂O and CO₂ co-reactants. Stochastic processes lead to the occasional deactivation of a given Pd cluster by the formation of a carbon overlayer. In such cases, supports with low but detectable rates of co-reactant activation, such as ZrO₂ or La₂O₃–ZrO₂, allow the ultimate removal of these overlayers and inhibit deactivation.

3.2. Effects of residence time and dilution on CH₄ reaction rates

Fig. 2 shows CH₄ reforming turnover rates (per surface Pd atom) at 823 K as a function of residence time on Pd/ZrO₂(1023) (1.6% wt.

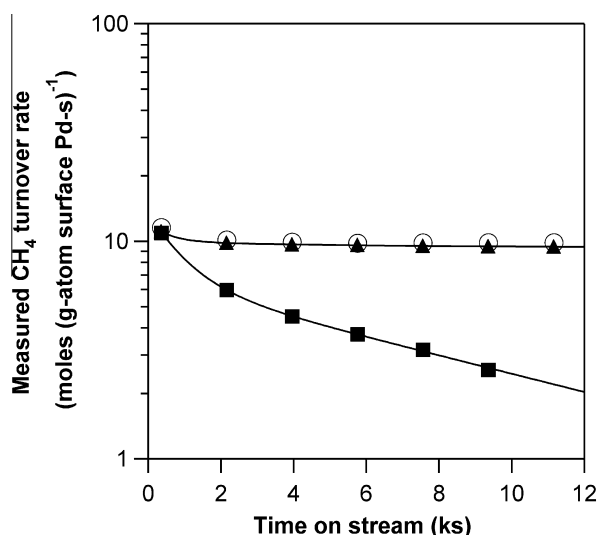


Fig. 1. Measured CH₄ turnover rates for CH₄–CO₂ reaction as a function of time on stream on (▲) 1.6% wt. Pd/ZrO₂(1023), (○) 1.6% wt. Pd/ZrO₂–La₂O₃(1023), and (■) 1.6% wt. Pd/Al₂O₃(1023) at 823 K ($P_{\text{CH}_4} = 10$ kPa, $P_{\text{CO}_2} = 40$ kPa, residence time 0.83 (10^6 cm³/g h)/Gas hourly space velocity).

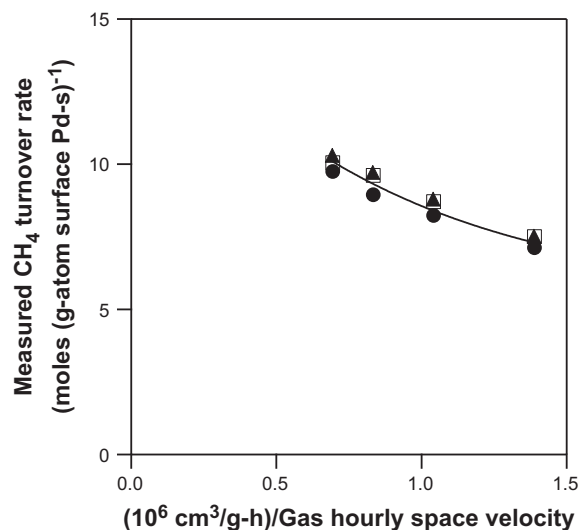


Fig. 2. Measured CH₄ reaction rates as a function of residence time for CH₄–CO₂ reaction on 1.6% wt. Pd/ZrO₂(1023) at 823 K ($P_{\text{CH}_4} = 10$ kPa, $P_{\text{CO}_2} = 40$ kPa, (●) 5 mg of catalyst diluted with 25 mg of Al₂O₃ (pellet size 250–425 μm), then diluted with 500 mg of ground quartz (250–425 μm), (▲) 5 mg of catalyst diluted with 50 mg of Al₂O₃ (250–425 μm), then diluted with 500 mg of ground quartz (250–425 μm), (○) 5 mg of catalyst diluted with 25 mg of Al₂O₃ (63–106 μm), then diluted with 500 mg of ground quartz (250–425 μm)).

Pd) catalysts with different pellet size (63–106 μm, 250–425 μm) and extent of dilution within pellets (γ -Al₂O₃:catalyst intrapellet dilution ratios = 5:1, 10:1) and within the catalyst bed (acid-washed quartz (250–425 μm); quartz:catalyst dilution ratio = 100:1). Neither pellet size nor intrapellet dilution influenced measured CH₄ turnover rates, indicating that rate data are unaffected by transport artifacts that cause ubiquitous temperature and concentration gradients; therefore, all measured rates strictly reflect the rates of chemical reactions at cluster surfaces.

Forward CH₄ turnover rates (r_f) were obtained from measured turnover rates (r_{net}) by correcting for the approach to equilibrium (η_i) for CH₄–CO₂ (Eq. (2)) and CH₄–H₂O (Eq. (3)) reactions [19]:

$$r_{f,i} = \frac{r_{\text{net},i}}{1 - \eta_i} \quad (1)$$

$$\eta_1 = \frac{[P_{\text{CO}}]^2 [P_{\text{H}_2}]^2}{[P_{\text{CH}_4}] [P_{\text{CO}_2}]} \times \frac{1}{K_1} \quad (2)$$

$$\eta_2 = \frac{[P_{\text{CO}}] [P_{\text{H}_2}]^3}{[P_{\text{CH}_4}] [P_{\text{H}_2\text{O}}]} \times \frac{1}{K_2} \quad (3)$$

[*P_j*] is the average pressure (in atm) of species *j* in the reactor, and *K*₁ and *K*₂ are equilibrium constants for CO₂ and H₂O reactions with CH₄, respectively [20]. The average pressures of reactants and products were used in all rate and equilibrium equations to correct for the small changes that occurred as conversion changed along the catalyst bed. At all conditions used in our experiments, η values were much smaller than unity for reactions with either CO₂ or H₂O, and CH₄ conversion levels were maintained below 9% in all experiments.

On other Group VIII metals (Ni, Ru, Rh, Pt, Ir) [5,6], forward CH₄ turnover rates (from Eq. (1)) did not depend on residence time or H₂ and CO product concentrations. In contrast, both measured (Fig. 2) and forward (Fig. S2) CH₄ reforming rates decreased with increasing residence time on Pd-based catalysts, even though CH₄ and co-reactant concentrations were essentially unaffected by residence time at the low conversions prevalent in these experiments. We conclude that these effects must reflect the inhibition of CH₄ reforming reactions by H₂ and/or CO reaction products.

The next sections provide evidence for these conclusions by probing the effects of added H₂ and CO and of reactant concentrations on reforming turnover rates.

3.3. Effect of reactant and product concentrations on CH₄ turnover rates

CH₄–CO₂ and CH₄–H₂O reaction rates on 1.6% wt. Pd/ZrO₂(1023) at 823 K are shown as a function of CH₄ pressure in Fig. 3. Forward CH₄ turnover rates increased with increasing CH₄ pressure, but non-linearly, for both reactions; turnover rates were also slightly higher with H₂O than with CO₂ co-reactants. On other metals (Ni, Ru, Rh, Pt, Ir) [5,6], forward CH₄ turnover rates were strictly proportional to CH₄ pressure but unaffected by the identity or concentration of the co-reactant. As we discuss below, these small differences in CH₄–CO₂ and CH₄–H₂O turnover rates on Pd-based catalysts reflect differences in the prevalent concentrations of CO and H₂ with these two co-reactants and their respective inhibitory effects on C–H bond activation rates.

Fig. 4 shows the effects of CO₂ and H₂O pressures on CH₄ turnover rates on 1.6% wt. Pd/ZrO₂(1023) at 823 K. CH₄ turnover rates did not depend on CO₂ or H₂O pressures. The small differences between CH₄–CO₂ and CH₄–H₂O turnover rates again reflect differences in the prevalent CO and H₂ pressures and their inhibitory effects on C–H bond activation, as shown below (Sections 3.3 and 3.4). These data indicate that co-reactant activation steps are faster than C–H bond activation and thus kinetically-irrelevant and that adsorbed species derived from these co-reactants are not present at any significant surface concentrations during steady-state catalysis.

Forward CH₄ turnover rates are shown as a function of H₂ pressure for CH₄–CO₂–H₂ reactants in Fig. 5. Turnover rates decreased from 10.8 to 2.7 s⁻¹ as H₂ pressures increased from 0.33 kPa to 7.8 kPa, consistent with the observed effects of residence time on reforming rates (Fig. 2). The effects of CO pressure on CH₄ reforming turnover rates were measured using CH₄–CO₂–CO reactants (Fig. 6). Turnover rates decreased from 10.3 to 3.9 s⁻¹ as CO pressures increased from 0.98 kPa to 5.2 kPa. CH₄–CO₂ turnover rates before and after CO co-feed were identical, indicating that these effects reflect reversible inhibition instead of irreversible deactivation of Pd surface sites by reaction products.

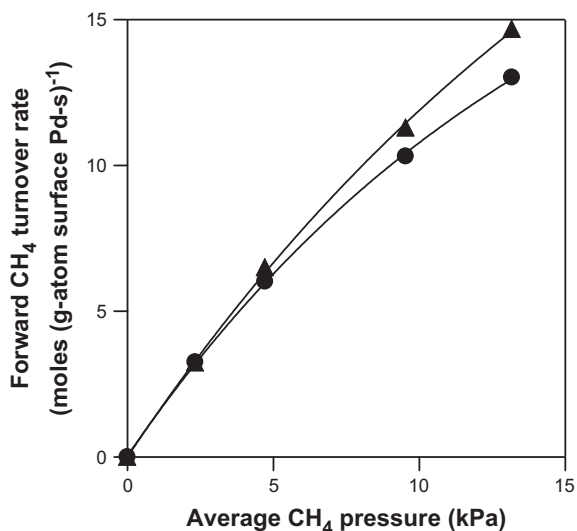


Fig. 3. Forward CH₄ turnover rates as a function of average CH₄ pressure for (●) CH₄–CO₂ and (▲) CH₄–H₂O reaction on 1.6% wt. Pd/ZrO₂(1023) at 823 K (P_{CO_2} or $P_{\text{H}_2\text{O}}$ = 40 kPa, residence time 0.83 (10⁶ cm³/g h)/Gas hourly space velocity).

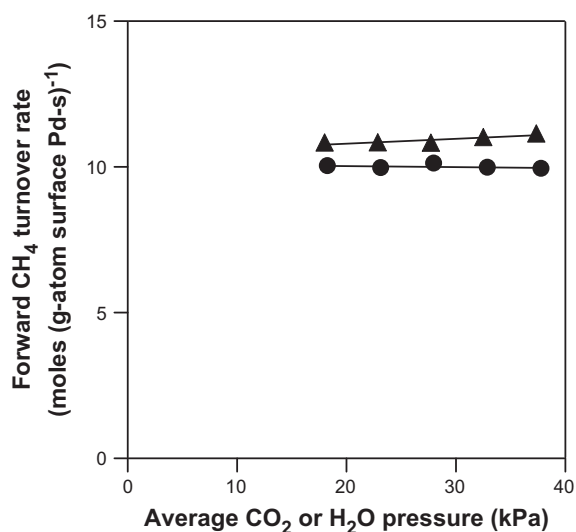


Fig. 4. Forward CH₄ turnover rates as a function of average (●) CO₂ or (▲) H₂O pressure for CH₄–CO₂ or CH₄–H₂O reaction on 1.6% wt. Pd/ZrO₂(1023) at 823 K (P_{CH_4} = 10 kPa, residence time 0.83 (10⁶ cm³/g h)/Gas hourly space velocity).

3.4. Kinetic isotope effects and isotopic tracing experiments

Table 2 shows H/D kinetic isotopic effects measured by comparing turnover rates with CH₄–CO₂, CD₄–CO₂, CH₄–H₂O, CD₄–H₂O, and CD₄–D₂O reactant mixtures (10 kPa CH₄ or CD₄, 40 kPa CO₂, H₂O or D₂O) on 1.6% wt. Pd/ZrO₂ at 823 K. The measured normal CH₄/CD₄ kinetic isotopic effects were identical for CO₂ or H₂O co-reactants (1.39–1.41). These data indicate that C–H bond activation is the only kinetically-relevant step on Pd clusters with both co-reactants. These similar kinetic isotope effects for CH₄/CD₄ with CO₂ and H₂O co-reactants also show that the extent to which this step controls overall reforming rates is independent of the identity of the co-reactant. No kinetic isotopic effects were observed for CD₄–D₂O and CD₄–H₂O reactants (0.97), consistent with the lack of kinetic relevance of water activation steps or of any steps involving water-derived intermediates. These kinetic isotopic effects on Pd catalysts are slightly smaller than typical values for other

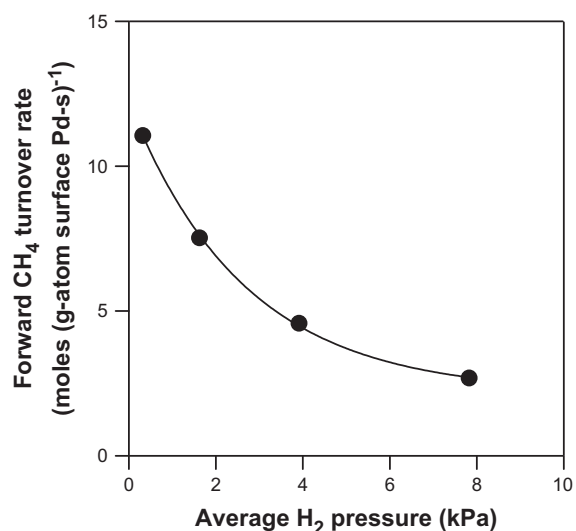


Fig. 5. Forward CH₄ turnover rates as a function of average H₂ pressure for CH₄–CO₂ reaction on 1.6% wt. Pd/ZrO₂(1023) at 823 K (P_{CH_4} = 10 kPa, P_{CO_2} = 40 kPa, residence time 0.83 (10⁶ cm³/g h)/Gas hourly space velocity).

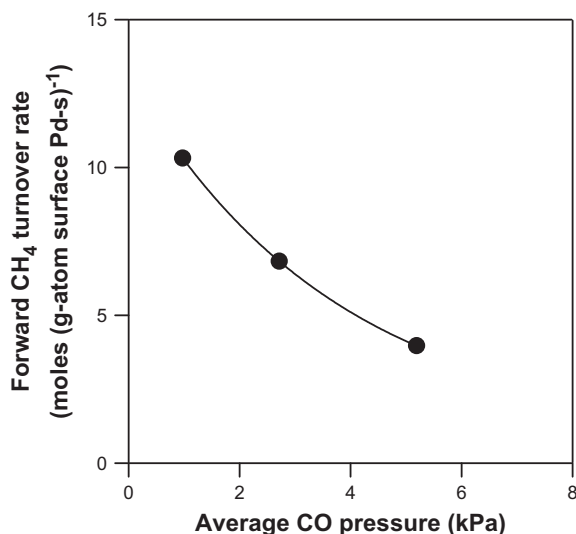


Fig. 6. Forward CH₄ turnover rates as a function of average CO pressure for CH₄–CO₂ reaction on 1.6% wt. Pd/ZrO₂(1023) at 823 K (P_{CH_4} = 10 kPa, P_{CO_2} = 40 kPa, residence time 0.83 (10⁶ cm³/g h)/Gas hourly space velocity).

Table 2

Kinetic isotope effects for CH₄ reactions on 1.6% wt. Pd/ZrO₂(1023) at 823 K (10 kPa CH₄ or CD₄, 40 kPa CO₂, H₂O, or D₂O) and on 1.6% wt. Pt/ZrO₂ at 873 K (25 kPa CH₄ or CD₄, 25 kPa CO₂, H₂O, or D₂O).

Catalysts	Pd/ZrO ₂ [This work]	Pt/ZrO ₂ [6]
$r(\text{CD}_4\text{-H}_2\text{O})/r(\text{CD}_4\text{-D}_2\text{O})$	0.97	1.07
$r(\text{CH}_4\text{-CO}_2)/r(\text{CD}_4\text{-CO}_2)$	1.41	1.77
$r(\text{CH}_4\text{-H}_2\text{O})/r(\text{CD}_4\text{-H}_2\text{O})$	1.39	1.69

metals (Pt (1.69–1.77 at 873 K) [6], Ir (1.75–1.81 at 873 K) [5], Ru (1.40–1.42 at 873 K) [6], Rh (1.54–1.56 at 873 K) [5], and Ni (1.62–1.66 at 873 K) [5]). These differences appear to reflect earlier transition states with shorter C–H bonds on the more reactive surfaces of Pd clusters, as suggested by theoretical treatments of the transition states involved in C–H bond activation steps on various metal surfaces [21].

CH₄–CO₂–D₂ reactant mixtures were used to determine whether inhibition reflects competitive co-adsorption leading to significant H⁺ coverages or the involvement of H-adatoms in reversing C–H bond activation steps. CH₄ chemical conversion rates were compared with the rate of formation of CH_{4-x}D_x isotopomers, measured by mass spectrometry (Table 3). CH₃D formation rates ($r(\text{CH}_3\text{D})$) were similar to those for chemical conversion of CH₄ to H₂ and CO ($r(\text{CO})$), indicating that CH₃^{*} and D⁺ (or H⁺) recombine often to form CH₃D (or CH₄) in the time scale of chemical conversion turnovers. Thus, we conclude that CH₄ activation steps leading to CH₃^{*} and H⁺ are reversible; in contrast, these steps were found to be irreversible and H₂ did not inhibit CH₄ reforming on

Table 3

Ratios of CH₃D formation rates ($r(\text{CH}_3\text{D})$) to CH₄ chemical conversion rates ($r(\text{CO})$) during reactions of CH₄–CO₂–D₂ mixture on 1.6% wt. Pd/ZrO₂(1023) at 823 K (P_{CH_4} = 10 kPa, P_{CO_2} = 40 kPa, residence time 0.83 (10⁶ cm³/g h)/Gas hourly space velocity).

Inlet D ₂ pressure (kPa)	$r(\text{CH}_3\text{D})/r(\text{CO})$
0	0
2	1.4
5	2.6
10	3.8

other Group VIII metals [5,6]. These differences among metals reflect, as we discuss in greater detail below, the larger C–H bond activation rate constants on Pd clusters compared with those on the other metals. CH₂D₂ and CHD₃ isotopomers formed at much lower rates (~20 times) than CH₃D, suggesting that subsequent C–H bond activation of CH₃^{*} species is essentially irreversible. The ratio of H/D scrambling to CH₄ chemical conversion rate ($\{r(\text{CH}_3\text{D})/r(\text{CO})\}$) increased with increasing D₂ pressure (Table 3), suggesting that CH₃D formation rates ($r(\text{CH}_3\text{D})$), via the microscopic reverse of the initial C–H bond activation step, increase with increasing concentrations of chemisorbed deuterium. This conclusion was confirmed by the linear dependence of the ($\{r(\text{CH}_3\text{D})/r(\text{CO})\}$) ratio on $P_{\text{D}_2}^{1/2}$ (Fig. S3); the latter dependence gives, in turn, the surface coverage of D⁺ for equilibrated adsorption–desorption steps.

The various dihydrogen isotopomers were present in binomial distributions at all conditions (e.g., H₂:HD:D₂, 0.046:0.30:0.65 vs. 0.044:0.33:0.63 for binomial; 10 kPa D₂), indicating that hydrogen dissociation–recombination steps are indeed at quasi-equilibrium during CH₄ reforming, even at the highest D₂ pressures and for CH₄ conversions far from thermodynamic equilibrium. The H⁺ coverages expected during reforming reactions were estimated from the heat of H₂ adsorption on Pd surfaces, reported to be 87 kJ mol⁻¹ on Pd(1 1 1) [22] and 102 kJ mol⁻¹ on Pd(1 1 0) [22]. These values would lead to H⁺ surface coverages much smaller than 0.01 on Pd surfaces at typical reaction conditions (823 K; 0.3–2 kPa H₂) and to desorption activation barriers (typically equal to adsorption heats for non-activated adsorption events) that would allow rapid adsorption–desorption equilibrium during reforming catalysis.

We conclude that initial C–H bond activation steps are reversible even when overall reforming reactions are essentially irreversible. The reversible nature of C–H bond activation elementary steps is responsible for the observed H₂ inhibition effects, which reflect the more frequent reversal of C–H activation events with increasing H₂ pressures and H⁺ concentrations.

3.5. Effect of CO on CH₄ reforming turnover rates

The expected CO coverages during reforming reactions were estimated from the heat of CO adsorption on Pd surfaces to consider whether inhibition could simply reflect competitive adsorption of CO or require its dissociative adsorption to form more strongly bound C⁺ and O⁺ species. The heat of CO molecular adsorption has been reported to be 140 kJ mol⁻¹ on Pd(1 1 1) [23], 170 kJ mol⁻¹ on Pd(1 1 0) [23], and 148 kJ mol⁻¹ on 1.5 to 9.5 nm Pd clusters [24]. These values would lead to CO surface coverages smaller than 0.1 on Pd surfaces for CH₄–CO₂ or CH₄–H₂O reactions at 823 K and typical CO pressures in our study (0.5–1 kPa). We conclude that molecularly adsorbed CO is unlikely to block Pd surface atoms to the extent required to cause the observed inhibition effects. Yet CH₄ turnover rates decreased markedly with increasing CO pressure (Fig. 6), apparently because of concurrent CO dissociation via the microscopic reverse of the recombination of C⁺ and O⁺, which forms the CO products of CH₄ reforming.

The reversible nature of CO dissociation steps was confirmed from the rate of isotopic scrambling of ¹²C¹⁶O(1 kPa)–¹³C¹⁸O(1 kPa) during ¹²CH₄(10 kPa)–¹²C¹⁶O₂(40 kPa) reactions at 823 K. Table 4 shows CO and CO₂ isotopomer concentrations in the effluent stream. ¹³C¹⁶O and ¹³C¹⁶O₂ isotopomers formed (via CO dissociation to C⁺ and O⁺ and subsequent recombination) at rates comparable to those for chemical conversion of CH₄ to CO (¹³C scrambling to CH₄ chemical conversion rate ratio ~0.17). CO isotopomers were not equilibrated (¹²C¹⁶O:¹²C¹⁸O:¹³C¹⁶O:¹³C¹⁸O, 0.78:0.013:0.070:0.13 vs. 0.70:0.12:0.17:0.030 for binomial distributions), indicating that CO dissociation steps are reversible but not quasi-equilibrated during CH₄ reforming. We conclude that CO inhibition of CH₄

Table 4

Isotopic distribution during $^{12}\text{C}^{16}\text{O}_2(40\text{ kPa})\text{--}^{13}\text{C}^{18}\text{O}(1\text{ kPa})\text{--}^{12}\text{C}^{16}\text{O}(1\text{ kPa})$ reaction on 1.6% wt. Pd/ZrO₂(1023) at 823 K (residence time 0.83 (10⁶ cm³/g h)/Gas hourly space velocity).

	<i>P</i> (kPa) in reactants	<i>P</i> (kPa) in products
$^{12}\text{C}^{16}\text{O}$	1.0	3.13
$^{12}\text{C}^{18}\text{O}$	0	0.051
$^{13}\text{C}^{16}\text{O}$	0	0.28
$^{13}\text{C}^{18}\text{O}$	1.0	0.53
$^{12}\text{C}^{16}\text{O}_2$	40.0	38.16
$^{12}\text{C}^{16}\text{O}^{18}\text{O}$	0	0.46
$^{12}\text{C}^{18}\text{O}_2$	0	0.0026
$^{13}\text{C}^{16}\text{O}_2$	0	0.31
$^{13}\text{C}^{16}\text{O}^{18}\text{O}$	0	0.013
$^{13}\text{C}^{18}\text{O}_2$	0	0

reforming reactions is caused by the formation of kinetically-detectable concentrations of active C* species via the microscopic reverse of the C*–O* recombination reactions that form CO during CH₄ reforming. These species decrease the number of unoccupied Pd sites (*) available for kinetically-relevant C–H activation steps and, as a result, the rate of the overall catalytic sequence. We show below that these conclusions are consistent with the form of the rate equation required to describe the effects of CO pressure on reaction rates.

3.6. Rates and mechanism for activation of CO₂ and H₂O co-reactants

H–D scrambling rates during reactions of CH₄(10 kPa)–D₂O (40 kPa) reactant mixtures were measured at 823 K from the effluent concentrations of CH_{4–x}D_x and H_{2–x}D_xO isotopomers during catalysis. CH₃D/CH₄ and HDO/D₂O ratios in the effluent were 0.014 and 0.029, respectively, while other isotopomers were not detected. Measured HDO/D₂O ratios (0.029) were significantly smaller than predicted from equilibrium between D₂O and the H-atoms (0.07) formed via CH₄ conversion and D₂O activation. These data indicate that water activation steps are not equilibrated during CH₄–H₂O reactions on Pd cluster surfaces. On other Group VIII metals (Ni, Ru, Rh, Pt, Ir) [5,6], H₂O activation steps were equilibrated and binomial isotopomer mixtures were formed from CH₄–H₂O–D₂ reactant mixtures.

The reversibility of CO₂ activation steps was determined from ¹³C exchange rates between CO₂ and CO in $^{12}\text{C}^{16}\text{O}_2(40\text{ kPa})\text{--}^{13}\text{C}^{16}\text{O}(5\text{ kPa})$ reactant mixtures. On other metals (Ni, Ru, Rh, Pt, and Ir) [5,6], these experiments led to identical ¹³C fractions in the CO and CO₂ molecules in the effluent even at very low CH₄ conversions; such rapid exchange indicates that CO₂–CO interconversion is much faster than chemical conversion of CH₄ and thus occurs in quasi-equilibrated steps on these other metals. In agreement with these data, the water–gas shift reaction, which involves H₂O and CO₂ activation steps, was also equilibrated at all reaction conditions on Ni, Ru, Rh, Pt, and Ir catalysts [5,6]. In contrast, the ¹³C fractions in CO and CO₂ molecules in the reactor effluent were 0.74 and 0.020, respectively, during $^{12}\text{C}^{16}\text{O}_2\text{--}^{13}\text{C}^{16}\text{O}$ reactions on Pd/ZrO₂. Thus, CO₂ activation steps that form CO* and O* are not quasi-equilibrated during CH₄–CO₂ reactions on Pd cluster surfaces, even at modest CH₄ chemical conversions (~7%). Water–gas shift and its reverse reaction also remained non-equilibrated ($\eta = 0.05\text{--}0.5$ for CH₄–CO₂ and CH₄–H₂O reactions) at all conditions, consistent with non-equilibrated CO₂ and H₂O activation elementary steps. The value of η was defined as:

$$\eta = \frac{[P_{\text{CO}}][P_{\text{H}_2\text{O}}]}{[P_{\text{CO}_2}][P_{\text{H}_2}]} \times \frac{1}{K_{\text{WGS}}} \quad (4)$$

where K_{WGS} is the equilibrium constant for the water–gas shift reaction.

3.7. Elementary steps involved in CH₄ reactions with H₂O and CO₂

We propose next a sequence of elementary steps (Scheme 1) consistent with the rate and isotopic data described in detail above. The reversibility of CH₄ activation steps (steps (5)–(8)) was confirmed from the rate of formation of CH_{4–x}D_x isotopomers during reactions of CH₄–CO₂–D₂ mixtures. The activation steps of co-reactants (step (9)–(11)) and the CO dissociation (step (12)) showed some reversibility but were not quasi-equilibrated during CH₄–CO₂ or CH₄–H₂O reactions on Pd clusters. Hydrogen dissociation–recombination steps (step (13)) were quasi-equilibrated during CH₄ reforming, as shown by the binomial dihydrogen isotopomer distribution obtained from CH₄–CO₂–D₂ reactant mixtures. Literature values [23,24] for CO adsorption enthalpies and CO desorption activation barriers (step (14)) indicate that molecular CO adsorption steps are quasi-equilibrated, but do not lead to significant CO* coverages, on Pd catalysts at the conditions of our CH₄ reforming experiments.

A rate equation for CH₄ conversion turnover rates (r_f) was derived from the sequence of elementary steps in Scheme 1 by applying the pseudo-steady-state hypothesis (PSSH) to [CH₃], [C*], [O*], and [OH*] adsorbed species (see Appendix I for details). PSSH for [CH₃*] gives:

$$[\text{CH}_3^*] = \frac{k_1[\text{CH}_4]}{k_{-1}\sqrt{\frac{[\text{H}_2]}{K_7}} + k_2} [*] \quad (15)$$

which taken together with the expression for the net rate of step (5) and the quasi-equilibrium equation for hydrogen dissociation (step (13)) gives an equation for the forward rate of CH₄ reforming:

$$r_f = k_1[\text{CH}_4][*]^2 - k_{-1}[\text{CH}_3^*][\text{H}^*] = k_2[\text{CH}_3^*][*] \\ = \frac{k_1[\text{CH}_4]}{\frac{k_{-1}}{k_2}\sqrt{\frac{[\text{H}_2]}{K_7}} + 1} [*]^2 = \alpha[*]^2 \quad (16)$$

$$\alpha = \frac{k_1[\text{CH}_4]}{\frac{k_{-1}}{k_2}\sqrt{\frac{[\text{H}_2]}{K_7}} + 1} \quad (17)$$

in terms of the concentration of unoccupied sites (*) present during steady-state catalysis. The concentration of unoccupied sites is given by the site balance:

$$[*] + [\text{C}^*] + [\text{O}^*] + [\text{CO}^*] = L \quad (18)$$

by evaluating the steady-state coverages of all other adsorbed intermediates. The [C*] term in Eq. (18) is given by its PSSH expression:

$$\alpha[*]^2 + k_6\frac{[\text{CO}]}{K_8}[*]^2 = k_{-6}[\text{C}^*][\text{O}^*] \quad (19)$$

A similar treatment for [OH*] gives:

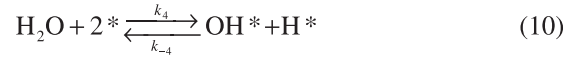
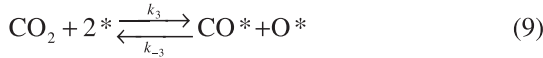
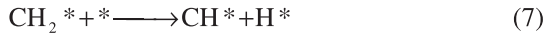
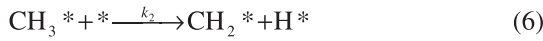
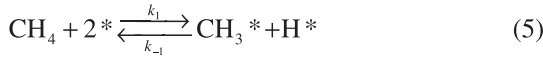
$$[\text{OH}^*] = \frac{\frac{k_4}{k_5}[\text{H}_2\text{O}][*] + \frac{k_{-5}}{k_5}\sqrt{\frac{[\text{H}_2]}{K_7}}[\text{O}^*]}{\frac{k_{-4}}{k_5}\sqrt{\frac{[\text{H}_2]}{K_7}} + 1} = \frac{\frac{k_4}{k_5}[\text{H}_2\text{O}][*] + \frac{k_{-5}}{k_5}\sqrt{\frac{[\text{H}_2]}{K_7}}[\text{O}^*]}{\beta} \quad (20)$$

where

$$\beta = \frac{k_{-4}}{k_5}\sqrt{\frac{[\text{H}_2]}{K_7}} + 1 \quad (21)$$

Finally, the PSSH assumption for [O*] gives the equation:

$$[\text{O}^*] = \frac{k_3[\text{CO}_2] + \frac{k_4}{\beta}[\text{H}_2\text{O}] - \alpha}{k_{-3}\frac{[\text{CO}]}{K_8} + k_{-5}\sqrt{\frac{[\text{H}_2]}{K_7}} - \frac{k_{-5}}{\beta}\sqrt{\frac{[\text{H}_2]}{K_7}}} [*] = \frac{\delta}{\gamma} [*] \quad (22)$$



Scheme 1. Sequence of elementary steps for CH₄ reforming reactions on Pd-based catalysts.

in which

$$\gamma = k_{-3} \frac{[\text{CO}]}{K_8} + k_{-5} \sqrt{\frac{[\text{H}_2]}{K_7}} - \frac{k_{-5}}{\beta} \sqrt{\frac{[\text{H}_2]}{K_7}} \quad (23)$$

$$\delta = k_3 [\text{CO}_2] + \frac{k_4}{\beta} [\text{H}_2\text{O}] - \alpha \quad (24)$$

The [C*] term can then be restated by combining Eqs. (19) and (22) to give:

$$[\text{C}^*] = \frac{\alpha + k_6 \frac{[\text{CO}]}{K_8}}{k_{-6} \frac{\delta}{\gamma}} [*] \quad (25)$$

The expressions for all adsorbed intermediates can be introduced into the site balance (Eq. (18)) to solve for the concentration of unoccupied sites:

$$[*] = \frac{1}{1 + \frac{\alpha + k_6 \frac{[\text{CO}]}{K_8}}{k_{-6} \frac{\delta}{\gamma}} + \frac{\delta}{\gamma} + \frac{[\text{CO}]}{K_8}} \quad (26)$$

The equation for the CH₄ turnover rate can then be obtained by substituting (*) into Eq. (16) to give:

$$r_f = \alpha [*]^2 = \frac{\alpha}{\left(1 + \frac{\alpha + k_6 \frac{[\text{CO}]}{K_8}}{k_{-6} \frac{\delta}{\gamma}} + \frac{\delta}{\gamma} + \frac{[\text{CO}]}{K_8}\right)^2} \quad (27)$$

Substituting the defining equation for α , β , γ , and δ into Eq. (27) gives a final equation for CH₄ reforming rates:

$$r_f = \frac{k_1 [\text{CH}_4]}{A \sqrt{[\text{H}_2]} + 1} \frac{1}{\left[1 + \left(\frac{k_1 [\text{CH}_4]}{A \sqrt{[\text{H}_2]} + 1}\right) \left(\frac{B[\text{CO}] + C \sqrt{[\text{H}_2]}}{D[\text{CO}_2] + E \frac{[\text{H}_2\text{O}]}{\sqrt{[\text{H}_2]}} - \frac{k_1 [\text{CH}_4]}{A \sqrt{[\text{H}_2]} + 1}}\right) + \left(\frac{[\text{CO}]}{K_8}\right)\right]^2} \quad (28)$$

in which all remaining parameters (k_1 , A , B , C , D , and E) consist only of rate and equilibrium constants for elementary steps without any residual concentration dependences, as shown in Table 5. In this final equation, k_1 is the rate constant for C–H bond activation in the elementary step (5) and K_8 is the equilibrium constant of CO adsorption and desorption steps (step (14)), and A , B , C , D , and E are constants composed of the rate constants and equilibrium constants shown in Scheme 1 (Table 5).

The underlying assumptions and the resulting functional form of this equation are consistent with all isotopic data and with the

observed product inhibition effects. This equation describes rates of CH₄ reactions with both H₂O and CO₂ as co-reactants, which lead, however, to different contributions from the various denominator terms in Eq. (28). These denominator terms correspond to the respective coverages of adsorbed species; their relative contributions can only be discerned by a rigorous comparison of all kinetic data with the form of Eq. (28).

We consider next a detailed analysis of all rate data in the context of Eq. (28) for three specific assumptions about the identity of the most abundant surface intermediates (MASI):

(i) CO* and * as MASI:

$$r_f = \frac{k_1 [\text{CH}_4]}{(A \sqrt{[\text{H}_2]} + 1) \left(\frac{[\text{CO}]}{K_8} + 1\right)^2} \quad (29)$$

(ii) O* and * as MASI:

$$r_f = \frac{k_1 [\text{CH}_4]}{A \sqrt{[\text{H}_2]} + 1} \frac{1}{\left[1 + \left(\frac{D[\text{CO}_2] + E \frac{[\text{H}_2\text{O}]}{\sqrt{[\text{H}_2]}} - \frac{k_1 [\text{CH}_4]}{A \sqrt{[\text{H}_2]} + 1}}{B[\text{CO}] + C \sqrt{[\text{H}_2]}}\right)\right]^2} \quad (30)$$

(iii) C* and * as MASI:

$$r_f = \frac{k_1 [\text{CH}_4]}{A \sqrt{[\text{H}_2]} + 1} \frac{1}{\left[1 + \left(\frac{k_1 [\text{CH}_4]}{A \sqrt{[\text{H}_2]} + 1}\right) \left(\frac{B[\text{CO}] + C \sqrt{[\text{H}_2]}}{D[\text{CO}_2] + E \frac{[\text{H}_2\text{O}]}{\sqrt{[\text{H}_2]}} - \frac{k_1 [\text{CH}_4]}{A \sqrt{[\text{H}_2]} + 1}}\right)\right]^2} \quad (31)$$

These three equations were compared with all rate data using linear regression analyses with minimization of residuals (Appen-

Table 5

Relations between kinetic parameters in Eq. (28) for CH₄–CO₂ and CH₄–H₂O reactions and rate and equilibrium constants for elementary steps.

Kinetic parameter	
A	$\frac{k_{-1}}{k_2} \sqrt{\frac{1}{K_7}}$
B	$\frac{k_{-3}}{K_8}$
C	$k_{-5} \sqrt{\frac{1}{K_7}}$
D	k_3
E	$\frac{k_4}{k_5} \sqrt{\frac{1}{K_7}}$

dix II). For O* and * as MASI, the values of B, or D and E in Eq. (30) were determined to be negative, indicating that such an assumption is inconsistent with the rate data. Indeed, Eq. (30) predicts that rates would increase with increasing CO pressure, in contradiction with the data in Fig. 6. We conclude that O* is not present at significant coverages during steady-state CH₄ reforming on Pd clusters.

Thus, we retain Eqs. (29) and (31) and estimate their respective parameters using all CH₄–CO₂ and CH₄–H₂O rate data at 823 K; their respective parity plots are shown in Fig. 7, and the resulting rate parameters are reported in Table 6. Eq. (31) provides a more accurate description of the rate data than Eq. (29) ($R^2 = 0.986$ vs. 0.952), indicating that C* and * are the MASI during CH₄ reforming reactions and that the inhibition effects of CO reflect its effect on C* coverages during catalysis. The choice of C* (instead of CO*) as the titrant for sites is consistent with the low CO* coverages expected from the heat of molecular adsorption of CO on Pd. Only three of the six kinetic parameters in Eq. (31) are required to describe the rate data (Supplementary material; Fig. S4). Forward CH₄ turnover rates for CH₄–CO₂ reactions are given by:

$$r_f = \frac{k_1[\text{CH}_4]}{(A\sqrt{[\text{H}_2]} + 1) \left(\frac{k_1[\text{CH}_4]}{(A\sqrt{[\text{H}_2]} + 1)} \frac{B}{D} \frac{[\text{CO}]}{[\text{CO}_2]} + 1 \right)^2},$$

$$A = \frac{k_{-1}}{k_2} \sqrt{\frac{1}{K_7}}, \quad B = \frac{k_{-3}}{k_3 K_8} \quad (32)$$

Forward CH₄ turnover rates for CH₄–H₂O reactions are given by:

$$r_f = \frac{k_1[\text{CH}_4]}{(A\sqrt{[\text{H}_2]} + 1) \left(\frac{k_1[\text{CH}_4]}{(A\sqrt{[\text{H}_2]} + 1)} \frac{B}{E} \frac{[\text{CO}]\sqrt{[\text{H}_2]}}{[\text{H}_2\text{O}]} + 1 \right)^2},$$

$$A = \frac{k_{-1}}{k_2} \sqrt{\frac{1}{K_7}}, \quad B = \frac{k_{-3}k_{-4}}{k_4 k_5 K_8} \sqrt{\frac{1}{K_7}} \quad (33)$$

The parameters for the best fit were estimated using the data of CH₄–CO₂ reactions for Eq. (32) and CH₄–H₂O reactions for Eq. (33) at 823 K separately. The parity plots are shown in Fig. 8 and the rate parameters in Table 6. Three parameters are used to fit the respective data to each of Eqs. (29), (32), and (33), but the goodness of fit was significantly better for Eqs. (32) and (33) ($R^2 = 0.975$ and 0.984) than for Eq. (29) ($R^2 = 0.952$), indicating that C* and * are the most plausible MASI during CH₄ reforming reactions.

These rate equations (Eq. (32) for CH₄–CO₂ and Eq. (33) for CH₄–H₂O) were used to estimate the relevant kinetic parameters from rate data at each temperature; the values of these parameters are shown in Table 7. Rate constants for C–H bond activation (k_1) and for the H₂ inhibition parameter (A) were similar whether

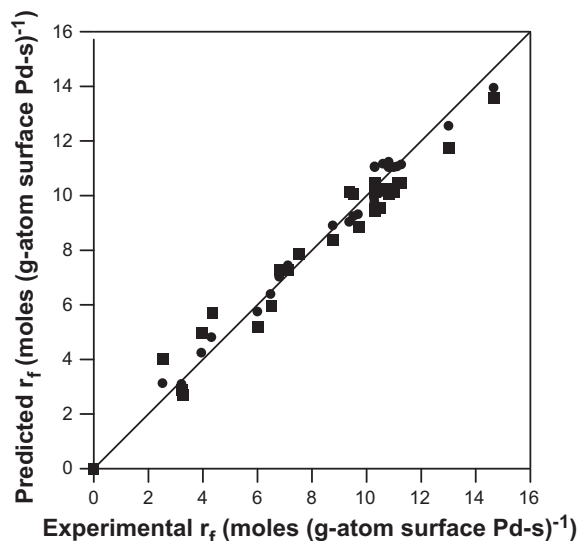


Fig. 7. Predicted experimental forward CH₄ turnover rates using (■) Eq. (29) and (●) Eq. (31) versus experimental forward CH₄ turnover rates for both CH₄–CO₂ and CH₄–H₂O reactions on 1.6% wt. Pd/ZrO₂(1023) at 823 K.

Table 6

Rate parameters of CH₄ reactions on 1.6% wt. Pd/ZrO₂(1023) for CH₄ reactions at 823 K and correlation coefficients for the rate equations.

Equation	Eq. (29) ^a	Eq. (31) ^a	Eq. (32) ^b	Eq. (33) ^c
k_1 (kPa ⁻¹ s ⁻¹)	2.3	1.7	1.9	2.1
A (kPa ^{-1/2})	0.92	0.74	1.2	1.1
B (kPa ⁻¹ s ⁻¹)	–	1.8	–	–
C (kPa ^{-1/2} s ⁻¹)	–	0.1	–	–
D (kPa ⁻¹ s ⁻¹)	–	5.6	–	–
E (kPa ^{-1/2} s ⁻¹)	–	5.3	–	–
K_8 (kPa)	4.3	–	–	–
B/D	–	–	0.30	–
B/E (kPa ^{-1/2})	–	–	–	0.41
R^2 (–)	0.952	0.986	0.975	0.984

^a Kinetic parameters from CH₄–CO₂ and CH₄–H₂O rate data.

^b Kinetic parameters from CH₄–CO₂ rate data.

^c Kinetic parameters from CH₄–H₂O rate data.

CH₄–CO₂ or CH₄–H₂O rate data were used in the regression (Table 7). These similar values indicate that neither CO₂ nor H₂O is involved in determining the magnitude of these two terms, consistent with Scheme 1, in which their respective values depend only on CH₄ dissociation and CH₃–H* recombination rates. The small differences in measured CO₂ and H₂O reforming rates (Fig. 4) reflect their respective roles in providing O* species at different rates; these O* species, even at their low prevalent surface coverages, act as the reactive scavengers that determine the concentration of the C* species formed via dissociation of both CH₄ and CO. The C* species from CH₄ and CO dissociation, which decrease in coverage with increasing concentration of O* formed in CO₂ and H₂O activation, represent the relevant C* in the denominator of Eqs. (32) and (33); as a result, CO₂ and H₂O influence the magnitude of this term and the severity of CO inhibition effects to different extents.

Fig. 9 shows Arrhenius plots for C–H bond activation rate constants with CO₂ and H₂O co-reactants (k_1 in Eqs. (32) and (33)) on 1.6% wt. Pd/ZrO₂(1023). Measured activation energies with CO₂ and H₂O are very similar (84 and 81 kJ mol⁻¹, respectively; Table 7), as expected from the identical kinetic origins of the two rate constants. These activation barriers are somewhat smaller than

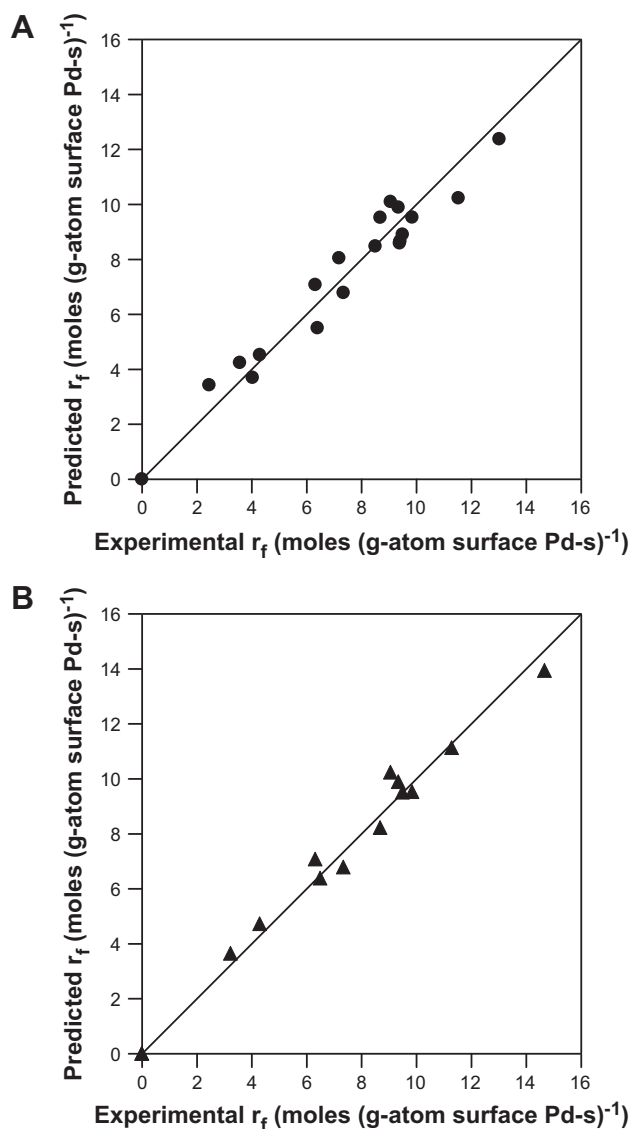


Fig. 8. Predicted experimental forward CH_4 turnover rates using (A) Eq. (32) for $\text{CH}_4\text{-CO}_2$ reaction and (B) Eq. (33) for $\text{CH}_4\text{-H}_2\text{O}$ reaction versus experimental forward CH_4 turnover rates for (A) $\text{CH}_4\text{-CO}_2$ and (B) $\text{CH}_4\text{-H}_2\text{O}$ reactions on 1.6% wt. Pd/ZrO₂(1023) at 823 K.

apparent activation energies reported previously from CO_2 reforming rate data without specific mechanistic analysis on 1% wt. Pd/Al₂O₃ (87.1 kJ mol⁻¹ [25] and 93.1 kJ mol⁻¹ [7]), 1% wt. Pd/TiO₂ (91.5 kJ mol⁻¹ [7]), 1% wt. Pd/CeO₂/Al₂O₃ (100 kJ mol⁻¹) [10], 1% wt. Pd/MgO (114 kJ mol⁻¹) [7], and 1% wt. Pd/SiO₂ (141 kJ mol⁻¹) [7]. These previous values may contain unintended effects of CO

and H₂ inhibition, deactivation consequences of temperature, and/or transport and thermodynamic artifacts. Our intrinsic barriers for C–H bond activation on Pd clusters are larger, however, than those estimated from density functional theory calculations on Pd(1 1 1) (63.7 kJ mol⁻¹), Pd-step (36.7 kJ mol⁻¹), and Pd-kink (39.6 kJ mol⁻¹) [18]. It seems plausible that such differences may reflect the strong binding of C* on corners and edges, which leads to their low activation barrier for C–H activation [21] and would render such highly active structures unable to turnover because of their permanent titration by C*. It is also conceivable that theoretical treatments underestimate C–H activation barriers because they neglect specific effects of clusters with significant atomic mobility and possibly containing trace amounts of dissolved carbon under typical conditions of reforming catalysis. We remark, however, that the experimental barriers reported here are those of CH_4 reactions, devoid of transport or thermodynamic corruptions, on Pd clusters as they exist at conditions relevant to CH_4 reforming catalysis.

3.8. Effects of Pd cluster size on CH_4 reforming turnover rates

Turnover rates were measured with $\text{CH}_4\text{-CO}_2$ and $\text{CH}_4\text{-H}_2\text{O}$ reactants at 923 K also on 1.6% wt. Pd/ZrO₂(1123) and 1.6% wt. Pd/ZrO₂-La₂O₃(1023) as a function of reactant and product concentrations. These samples gave smaller Pd dispersions (3.5% and 5.3%, respectively) than the 1.6% wt. Pd/ZrO₂(1023) (8.9%) sample for which detailed kinetic data were presented in earlier sections.

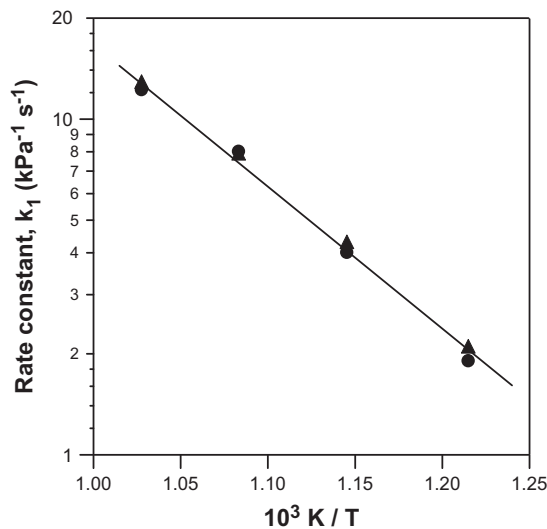


Fig. 9. Arrhenius plots for (●) $\text{CH}_4\text{-CO}_2$ and (▲) $\text{CH}_4\text{-H}_2\text{O}$ reactions of the rate constants, k_1 , for C–H bond activation on 1.6% wt. Pd/ZrO₂(1023).

Table 7
Kinetic parameters of CH_4 reactions on 1.6% wt. Pd/ZrO₂(1023) for $\text{CH}_4\text{-CO}_2$ and $\text{CH}_4\text{-H}_2\text{O}$ reactions.

Co-reactant	CO_2^a				H_2O^b			
Temperature (K)	823	873	923	973	823	873	923	973
k_1 (kPa ⁻¹ s ⁻¹)	1.9	4.0	8.0	12.2	2.1	4.3	7.9	12.9
A (kPa ^{-1/2})	1.2	1.0	0.51	0.19	1.1	1.0	0.52	0.18
B/D	0.30	0.29	0.17	0.14	–	–	–	–
B/E (kPa ^{-1/2})	–	–	–	–	0.41	0.35	0.22	0.19
Activation energy (kJ mol ⁻¹)	84 ± 4				81 ± 3			
Pre-exponential factor (10 ⁵ s ⁻¹ kPa ⁻¹)	4 ± 2				3 ± 1			

^a Parameters defined in Eq. (32).

^b Parameters defined in Eq. (33).

Table 8

Kinetic parameters of CH₄ reactions on Pd/ZrO₂(1123), Pd/ZrO₂-La₂O₃(1023), and Pd/ZrO₂(1023) (1.6% wt. Pd) at 923 K for CH₄-CO₂ and CH₄-H₂O reactions.

Catalyst	Pd/ZrO ₂ (1123)		Pd/ZrO ₂ -La ₂ O ₃ (1023)		Pd/ZrO ₂ (1023)	
	CO ₂ ^a	H ₂ O ^b	CO ₂ ^a	H ₂ O ^b	CO ₂ ^a	H ₂ O ^b
<i>k</i> ₁ (kPa ⁻¹ s ⁻¹)	7.8	8.0	8.1	7.8	8.0	7.9
<i>A</i> (kPa ^{-1/2})	0.49	0.54	0.52	0.50	0.51	0.52
<i>B/D</i>	0.16	–	0.17	–	0.17	–
<i>B/E</i> (kPa ^{-1/2})	–	0.25	–	0.23	–	0.22

^a Parameters defined in Eq. (32).

^b Parameters defined in Eq. (33).

These data and their kinetic analysis were used to probe the consequences of Pd cluster size on the rate constant for C–H bond activation.

Rate data on these three catalysts were accurately described by Eq. (32) for CH₄-CO₂ reactions and Eq. (33) for CH₄-H₂O reactions, and the rate constants (*k*₁) for C–H bond activation and inhibition parameters are shown in Table 8 for all three samples. The C–H bond activation rate constants did not vary with Pd dispersion (3.5–8.9%) within experimental accuracy (Table 8), in spite of a monotonic increase in the fraction of exposed surface Pd atoms at corner and edge location with increasing Pd dispersion [16]. Such insensitivity to structure, which contrasts the small increase in C–H bond activation rates with increasing dispersion for other metals (Fig. 10) [6], appears to reflect the predominant contributions of low-index planes on large Pd clusters to measured rates and the difficulty in stabilizing small Pd metal clusters against sintering at reforming reaction temperatures. Such low-index surfaces prevail on large clusters and exhibit much higher reactivity than on the other metals, apparently because of a concomitant stronger binding of C* on Pd compared with that on other metals. Such higher C* binding energies, evident from CO inhibition effects that were not evident on other Group VIII metals [5,6], make contributions from edge and corner sites even less likely than on the other metals, as a result of their irreversible titration by C* species more strongly bound on corners and edges than on low-index planes.

Supports (ZrO₂ and ZrO₂-La₂O₃) did not influence the rate constant for C–H bond activation or the H₂ inhibition parameter (Table 8), consistent with the proposal that all elementary steps in Scheme 1 proceed on Pd cluster surfaces. Detailed kinetic data are not available on 1.6% wt. Pd/Al₂O₃(1023) because of difficulties imposed by its less stable reforming rates (Fig. 1). A value for the C–H bond activation rate constant can be estimated, however, from initial reforming turnover rates (extrapolated to zero time-on-stream) by correcting these rates for the (small) effects H₂ and CO pressures using the values of *A* (1.2 kPa^{-1/2}) and *B/D* (0.30) (Table 7, Fig. S5). The value obtained for *k*₁ on Pd/Al₂O₃(1023) was 2.5 kPa⁻¹ s⁻¹ at 823 K, which is quite similar to that measured on Pd/ZrO₂(1023) (1.9 kPa⁻¹ s⁻¹) at the same temperature.

The *k*₁ values for C–H bond activation steps at 873 K (4.0 and 4.3 kPa⁻¹ s⁻¹, with CO₂ and H₂O, respectively) on 1.6% wt. Pd/ZrO₂(1023) are four times larger than the highest values measured on any other Group VIII catalysts [5,6] (Fig. 10) and more than 10 times larger than turnover rates extrapolated to the same dispersion of the Pd samples on the other metals. The high activity of Pd surfaces for C–H bond activation leads to the rapid formation of C*, which scavenges active O* species from co-reactants and prevents the equilibration of their activation steps on Pd surfaces and leads to reversibility for both C–H activation and C–O formation steps. The reactivity of Pd surfaces in C–H activation and their tendency to be inhibited by C* during reforming appear to reflect their strong affinity for C*, which can lead to significant deactivations and to bifunctional effects of support when reforming experiments are conducted at low H₂O/CH₄ or CO₂/CH₄ reactant ratios.

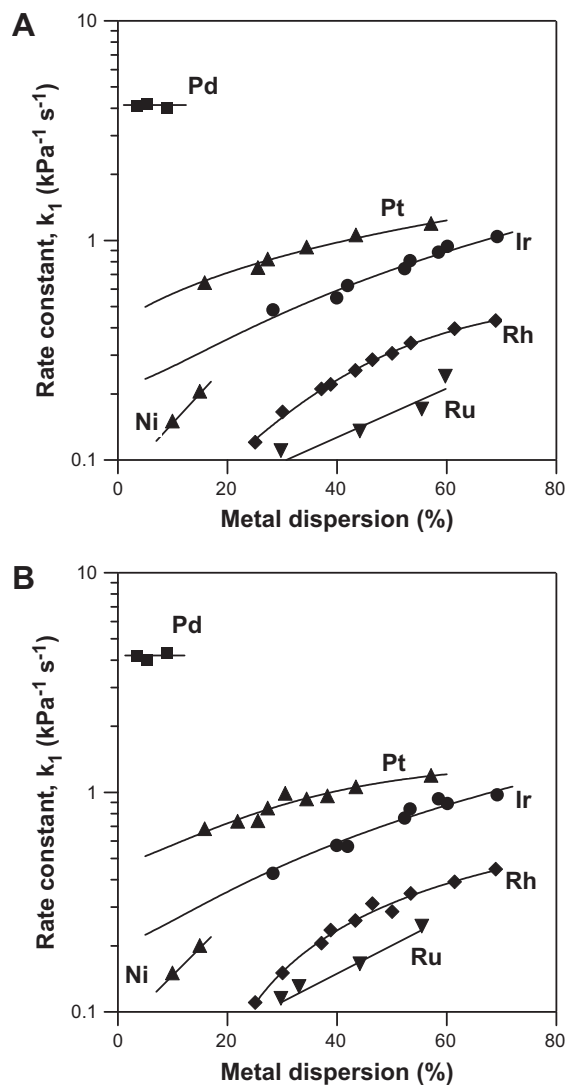


Fig. 10. Rate constants for C–H bond activation in CH₄ for (A) CO₂ and (B) H₂O reforming of CH₄ at 873 K on different metal clusters as a function of metal dispersion. The data for Ni, Ru, Rh, Ir, and Pt have been previously reported [5,6].

4. Conclusions

A reaction mechanism and a detailed sequence of elementary steps required for CO₂ or H₂O reforming of CH₄ on supported Pd catalysts were investigated by kinetic and isotopic tracer studies. The initial C–H bond activation step is reversible during CH₄ reforming reaction on Pd clusters even when overall reforming reactions are far from equilibrium, a conclusion confirmed by rates of formation of CH₃D isotopomers from CH₄-CO₂-D₂ mixtures that are similar to those for chemical conversion. On other Group VIII metals, C–H bond activation steps are irreversible and H₂ does not inhibit CH₄ reforming reactions. CO₂ and H₂O activation steps are not quasi-equilibrated during CH₄-CO₂ and CH₄-H₂O reactions on Pd clusters, consistent with the slow isotopic exchange between CO and CO₂ in CH₄-CO₂-¹³C mixtures and with the low HDO/D₂O ratio during reactions of CH₄-D₂O mixtures. Water-gas shift reactions also remained non-equilibrated during CH₄-CO₂ and CH₄-H₂O reactions, as expected from the irreversible nature of CO₂ and H₂O activation steps. CO dissociation steps (to C* and O*) are reversible but not quasi-equilibrated during CH₄ reforming reactions, as shown from the ¹³C content in CO and CO₂ during ¹²CH₄-¹²C¹⁶O₂-¹²C¹⁶O-¹³C¹⁸O reactions. These

kinetic and isotopic results on Pd clusters are consistent with a sequence of elementary steps similar to that proposed on other Group VIII metals. The resulting rate equation accurately describes measured rates and indicates that chemisorbed carbon (C*) and unoccupied Pd atoms (*) are the most abundant surface intermediates. First-order rate constants, corresponding to C–H bond activation steps, are ~10-fold larger than on all other Group VIII metals. This high reactivity of Pd surfaces causes this step to become reversible, leading to inhibition effects by H₂ mediated by its microscopic reverse and by C* species introduced as a result of the reversible nature of both CO and CH₄ dissociation steps. The reactive nature of Pd surface atoms appears to reflect their strong affinity for both C and H atoms formed in CH₄ activation steps, which lead to more stable transition states for the initial C–H bond activation. The catalytic consequences of Pd cluster size are quite weak over the limited range of Pd dispersion accessible at typical conditions of CH₄ reforming. Supports did not influence C–H bond activation or reforming turnover rates, but those supports with low but detectable reactivity in the activation of co-reactants were able to reverse the infrequent blockage of clusters surfaces by carbon overlayers, thus inhibiting deactivation.

Acknowledgments

This study was supported by BP as part of the Methane Conversion Cooperative Research Program at the University of California at Berkeley. We acknowledge Dr. Theo Fleisch (BP), Dr. Junmei Wei and Ms. Cathy Chin (UC-Berkeley) for helpful technical discussions. Transmission electron micrographs were kindly provided by Professor Miguel Avalos Borja of the Centro de Ciencias de la Materia Condensada of the Universidad Nacional Autonoma de Mexico.

Appendix I

A sequence of elementary steps for CH₄ reforming reactions on Pd-based catalysts is shown in Scheme 1. The steps (13) and (14) give following formulas.

$$[H^*] = \sqrt{\frac{[H_2]}{K_7}} [*] \quad (A1)$$

$$[CO^*] = \frac{[CO][*]}{K_8} \quad (A2)$$

The pseudo-steady-state hypothesis (PSSH) is applied to [CH₃*].

$$k_1[CH_4][*]^2 = k_{-1}[CH_3^*][H^*] + k_2[CH_3^*][*] \quad (A3)$$

$$[CH_3^*] = \frac{k_1[CH_4]}{k_{-1}\sqrt{\frac{[H_2]}{K_7}} + k_2} [*] \quad (A4)$$

Forward CH₄ turnover rates in step (5) are expressed by the following formula.

$$\begin{aligned} r_f &= k_1[CH_4][*]^2 - k_{-1}[CH_3^*][H^*] = k_2[CH_3^*][*] \\ &= \frac{k_1[CH_4]}{\frac{k_{-1}}{k_2}\sqrt{\frac{[H_2]}{K_7}} + 1} [*]^2 = \alpha[*]^2 \end{aligned} \quad (A5)$$

in which

$$\alpha = \frac{k_1[CH_4]}{\frac{k_{-1}}{k_2}\sqrt{\frac{[H_2]}{K_7}} + 1} \quad (A6)$$

The concentration of free sites (*) can be derived from the site balance equation:

$$[*] + [C^*] + [O^*] + [CO^*] = L \quad (A7)$$

by evaluating the steady-state coverages of the various adsorbed intermediates. The PSSH is applied to [C*].

$$k_2[CH_3^*][*] + k_6[CO^*][*] = k_{-6}[C^*][O^*] \quad (A8)$$

$$\alpha[*]^2 + k_6\frac{[CO]}{K_8}[*]^2 = k_{-6}[C^*][O^*] \quad (A9)$$

The PSSH is also applied to [OH*].

$$k_4[H_2O][*]^2 + k_{-5}[H^*][O^*] = k_{-4}[OH^*][H^*] + k_5[OH^*][*] \quad (A10)$$

$$[OH^*] \left(k_{-4}\sqrt{\frac{[H_2]}{K_7}} + k_5 \right) = k_4[H_2O][*] + k_{-5}\sqrt{\frac{[H_2]}{K_7}}[O^*] \quad (A11)$$

$$[OH^*] = \frac{\frac{k_4}{k_5}[H_2O][*] + \frac{k_{-5}}{k_5}\sqrt{\frac{[H_2]}{K_7}}[O^*]}{\frac{k_{-4}}{k_5}\sqrt{\frac{[H_2]}{K_7}} + 1} = \frac{\frac{k_4}{k_5}[H_2O][*] + \frac{k_{-5}}{k_5}\sqrt{\frac{[H_2]}{K_7}}[O^*]}{\beta} \quad (A12)$$

in which

$$\beta = \frac{k_{-4}}{k_5}\sqrt{\frac{[H_2]}{K_7}} + 1 \quad (A13)$$

The PSSH equation for [O*] gives the equation.

$$k_3[CO_2][*]^2 + k_5[OH^*][*] + k_6[CO^*][*] = k_{-3}[CO^*][O^*] + k_{-5}[H^*][O^*] + k_{-6}[C^*][O^*] \quad (A14)$$

$$k_3[CO_2][*]^2 + \frac{k_4}{\beta}[H_2O][*]^2 + \frac{k_{-5}}{\beta}\sqrt{\frac{[H_2]}{K_7}}[O^*][*] = k_{-3}\frac{[CO][*]}{K_8}[O^*] + k_{-5}\sqrt{\frac{[H_2]}{K_7}}[*][O^*] + \alpha[*]^2 \quad (A15)$$

$$\begin{aligned} [O^*] &\left(k_{-3}\frac{[CO]}{K_8} + k_{-5}\sqrt{\frac{[H_2]}{K_7}} - \frac{k_{-5}}{\beta}\sqrt{\frac{[H_2]}{K_7}} \right) \\ &= [*] \left(k_3[CO_2] + \frac{k_4}{\beta}[H_2O] - \alpha \right) \end{aligned} \quad (A16)$$

$$[O^*] = \frac{k_3[CO_2] + \frac{k_4}{\beta}[H_2O] - \alpha}{k_{-3}\frac{[CO]}{K_8} + k_{-5}\sqrt{\frac{[H_2]}{K_7}} - \frac{k_{-5}}{\beta}\sqrt{\frac{[H_2]}{K_7}}} [*] = \frac{\delta}{\gamma} [*] \quad (A17)$$

in which

$$\gamma = k_{-3}\frac{[CO]}{K_8} + k_{-5}\sqrt{\frac{[H_2]}{K_7}} - \frac{k_{-5}}{\beta}\sqrt{\frac{[H_2]}{K_7}} \quad (A18)$$

$$\delta = k_3[CO_2] + \frac{k_4}{\beta}[H_2O] - \alpha \quad (A19)$$

Eq. (A9) can be rewritten by the following equation using Eq. (A17).

$$\alpha[*]^2 + k_6\frac{[CO]}{K_8}[*]^2 = k_{-6}\frac{\delta}{\gamma}[C^*][*] \quad (A20)$$

$$[C^*] = \frac{\alpha + k_6\frac{[CO]}{K_8}}{k_{-6}\frac{\delta}{\gamma}} [*] \quad (A21)$$

Using Eqs. (A2), (A7), (A17), and (A21), we can obtain the following formula.

$$[*] = \frac{1}{1 + \frac{\alpha + k_6\frac{[CO]}{K_8}}{k_{-6}\frac{\delta}{\gamma}} + \frac{\delta}{\gamma} + \frac{[CO]}{K_8}} \quad (A22)$$

Forward CH₄ turnover rates are expressed by the following formula using Eq. (A5).

$$r_f = \alpha[*]^2 = \frac{\alpha}{\left(1 + \frac{\alpha + k_6\frac{[CO]}{K_8}}{k_{-6}\frac{\delta}{\gamma}} + \frac{\delta}{\gamma} + \frac{[CO]}{K_8} \right)^2} \quad (A23)$$

We conclude that $\alpha \gg k_6\frac{[CO]}{K_8}$, because CH₃* decomposition (α) is much faster than CO dissociation ($k_6\frac{[CO]}{K_8}$), as shown by the small

extent of isotopic scrambling in $^{12}\text{C}^{16}\text{O}$ – $^{13}\text{C}^{18}\text{O}$ mixtures during CH_4 – CO_2 reactions.

The goodness of fit was assessed from the respective correlation coefficients (R).

$$R = \frac{\sum_{i=1}^n (r_f(\text{experimental})_i - r_f(\text{experimental})_{\text{av}})(r_f(\text{predicted})_i - r_f(\text{predicted})_{\text{av}})}{\sqrt{\sum_{i=1}^n (r_f(\text{experimental})_i - r_f(\text{experimental})_{\text{av}})^2} \sqrt{\sum_{i=1}^n (r_f(\text{predicted})_i - r_f(\text{predicted})_{\text{av}})^2}} \quad (\text{A33})$$

$$r_f = \frac{\alpha}{\left(1 + \frac{\alpha}{k_{-6}\beta} + \frac{\delta}{\gamma} + \frac{[\text{CO}]}{K_8}\right)^2} \quad (\text{A24})$$

in which

$$\alpha = \frac{k_1[\text{CH}_4]}{\frac{k_{-1}}{k_2} \sqrt{\frac{[\text{H}_2]}{K_7}} + 1} = \frac{k_1[\text{CH}_4]}{A\sqrt{[\text{H}_2]} + 1} \quad (\text{A25})$$

$$\beta = \frac{k_{-4}}{k_5} \sqrt{\frac{[\text{H}_2]}{K_7}} + 1 \quad (\text{A26})$$

$$\gamma = k_{-3} \frac{[\text{CO}]}{K_8} + k_{-5} \sqrt{\frac{[\text{H}_2]}{K_7}} - \frac{k_{-5}}{\beta} \sqrt{\frac{[\text{H}_2]}{K_7}} = k_{-3} \frac{[\text{CO}]}{K_8} + k_{-5} \sqrt{\frac{[\text{H}_2]}{K_7}} \left(1 - \frac{1}{\frac{k_{-4}}{k_5} \sqrt{\frac{[\text{H}_2]}{K_7}} + 1}\right) \quad (\text{A27})$$

$$\delta = k_3[\text{CO}_2] + \frac{k_4}{\beta}[\text{H}_2\text{O}] - \alpha = k_3[\text{CO}_2] + \frac{k_4}{\frac{k_{-4}}{k_5} \sqrt{\frac{[\text{H}_2]}{K_7}} + 1}[\text{H}_2\text{O}] - \frac{k_1[\text{CH}_4]}{A\sqrt{[\text{H}_2]} + 1} \quad (\text{A28})$$

When $\frac{k_{-4}}{k_5} \sqrt{\frac{[\text{H}_2]}{K_7}} \gg 1$,

$$\gamma \approx k_{-3} \frac{[\text{CO}]}{K_8} + k_{-5} \sqrt{\frac{[\text{H}_2]}{K_7}} = B[\text{CO}] + C\sqrt{[\text{H}_2]} \quad (\text{A29})$$

$$\begin{aligned} \delta &\approx k_3[\text{CO}_2] + \frac{k_4}{\frac{k_{-4}}{k_5} \sqrt{\frac{[\text{H}_2]}{K_7}}}[\text{H}_2\text{O}] - \frac{k_1[\text{CH}_4]}{A\sqrt{[\text{H}_2]} + 1} \\ &= D[\text{CO}_2] + E \frac{[\text{H}_2\text{O}]}{\sqrt{[\text{H}_2]}} - \frac{k_1[\text{CH}_4]}{A\sqrt{[\text{H}_2]} + 1} \end{aligned} \quad (\text{A30})$$

Forward CH_4 turnover rates are expressed by the following formula using the parameters (k_1 , K_8 , A , B , C , D , and E), which do not contain any residual dependences on concentrations of reactants and products.

$$r_f = \frac{\frac{k_1[\text{CH}_4]}{A\sqrt{[\text{H}_2]} + 1}}{\left[1 + \left(\frac{k_1[\text{CH}_4]}{A\sqrt{[\text{H}_2]} + 1}\right) \left(\frac{B[\text{CO}] + C\sqrt{[\text{H}_2]}}{D[\text{CO}_2] + E \frac{[\text{H}_2\text{O}]}{\sqrt{[\text{H}_2]}} + \frac{k_1[\text{CH}_4]}{A\sqrt{[\text{H}_2]} + 1}}\right) + \left(\frac{D[\text{CO}_2] + E \frac{[\text{H}_2\text{O}]}{\sqrt{[\text{H}_2]}} + \frac{k_1[\text{CH}_4]}{A\sqrt{[\text{H}_2]} + 1}}{B[\text{CO}] + C\sqrt{[\text{H}_2]}}\right) + \left(\frac{[\text{CO}]}{K_8}\right)\right]^2} \quad (\text{A31})$$

In this final equation, k_1 is the rate constant for C–H bond activation in the elementary step (5) and K_8 is the equilibrium constant of CO adsorption and desorption steps (step (14)), and A , B , C , D , and E are constants composed of the rate constants and equilibrium constants shown in Scheme 1.

Appendix II

Rate parameters were determined using linear regression analyses with minimization of residuals (S):

$$S = \sum_{i=1}^n (r_f(\text{experimental})_i - r_f(\text{predicted})_i)^2 \quad (\text{A32})$$

In these equations, $r_f(\text{experimental})_{\text{av}}$ and $r_f(\text{predicted})_{\text{av}}$ are average values of $r_f(\text{experimental})$ and $r_f(\text{predicted})$, respectively.

Appendix C. Supplementary material

Supplementary data associated with this article can be found, in the online version, at doi:10.1016/j.jcat.2010.06.001.

References

- [1] S. Wang, G.Q.M. Lu, G.J. Millar, *Energy Fuels* 10 (1996) 896–904; T. Inui, *Appl. Oranometal. Chem.* 15 (2001) 87–94.
- [2] M.C.J. Bradford, M.A. Vannice, *Catal. Rev. Sci. Eng.* 41 (1999) 1–42.
- [3] K.P. De Jong, J.W. Geus, *Catal. Rev. Sci. Eng.* 42 (2000) 481–510; L. Dussault, J.C. Dupin, C. Guimon, M. Monthieux, N. Latorre, T. Ubierto, E. Romeo, C. Royo, A. Monzon, *J. Catal.* 251 (2007) 223–232; I. Kvande, D. Chen, Z. Yu, M. Ronning, A. Holmen, *J. Catal.* 256 (2008) 204–214.
- [4] S.J. Blanksby, G.B. Ellison, *Acc. Chem. Res.* 36 (2003) 255–263.
- [5] J. Wei, E. Iglesia, *Angew. Chem. Int. Ed.* 43 (2004) 3685–3688; J. Wei, E. Iglesia, *Phys. Chem. Chem. Phys.* 6 (2004) 3754–3759; J. Wei, E. Iglesia, *J. Catal.* 225 (2004) 116–127; J. Wei, E. Iglesia, *J. Catal.* 224 (2004) 370–383.
- [6] J. Wei, E. Iglesia, *J. Phys. Chem. B* 108 (2004) 7253–7262; J. Wei, E. Iglesia, *J. Phys. Chem. B* 108 (2004) 4094–4103.
- [7] A. Erdohelyi, J. Cserenyi, E. Papp, *F. Solymosi, Appl. Catal. A* 108 (1994) 205–219.
- [8] K. Nagaoka, K. Aika, *Bull. Chem. Soc. Jpn.* 74 (2001) 1841–1846.
- [9] R. Craciun, W. Daniell, H. Knozinger, *Appl. Catal. A* 230 (2002) 153–168.
- [10] P.G. Schulz, M.G. Gonzalez, C.E. Quincoces, C.E. Gigola, *Ind. Eng. Chem. Res.* 44 (2005) 9020–9029.
- [11] C.E. Gigola, M.S. Moreno, I. Costilla, M.D. Sanchez, *Appl. Surf. Sci.* 254 (2007) 325–329; L.S.F. Feio, C.E. Hori, S. Damyanova, F.B. Noronha, W.H. Cassinelli, C.M.P. Marques, J.M.C. Bueno, *Appl. Catal. A* 316 (2007) 107–116; W.H. Cassinelli, L.S.F. Feio, J.C.S. Araujo, C.E. Hori, F.B. Noronha, C.M.P. Marques, J.M.C. Bueno, *Catal. Lett.* 120 (2008) 86–94.
- [12] T. Osaki, T. Horiuchi, K. Suzuki, T. Mori, *Catal. Lett.* 44 (1997) 19–21; Z. Zhang, X.E. Verykios, *Catal. Lett.* 38 (1996) 175–179; H.-Y. Wang, C.-T. Au, *Catal. Lett.* 38 (1996) 77–79.
- [13] J.E. Benson, H.S. Hwang, M. Boudart, *J. Catal.* 30 (1973) 146–153.
- [14] G.L. Price, E. Iglesia, *Ind. Eng. Chem. Res.* 28 (1989) 839–844.
- [15] R.-J. Liu, P.A. Crozier, C.M. Smith, D.A. Hucul, J. Blackson, G. Salaita, *Appl. Catal. A* 282 (2005) 111–121; M.S. Moreno, F. Wang, M. Malac, T. Kasama, C.E. Gigola, I. Costilla, M.D. Sanchez, *J. Appl. Phys.* 105 (2009) 083531.
- [16] R. Van Hardeveld, F. Hartog, *Surf. Sci.* 15 (1969) 189–230.
- [17] K. Klier, J.S. Hess, R.G. Herman, *J. Chem. Phys.* 107 (1997) 4033–4043; G. Jones, J.G. Jakobsen, S.S. Shim, J. Kleis, M.P. Andersson, J. Rossmel, F. Abild-Pedersen, T. Bligaard, S. Helveg, B. Hinnemann, J.R. Rostrup-Nielsen, I. Chorkendorff, J. Sehested, J.K. Norskov, *J. Catal.* 259 (2008) 147–160.
- [18] Z.-P. Liu, P. Hu, *J. Am. Chem. Soc.* 125 (2003) 1958–1967.
- [19] M. Boudart, G. Djega-Mariadasson, *Kinetics of Heterogeneous Catalytic Reactions*, Princeton University Press, Princeton, NJ, 1984.
- [20] D.R. Stull, E.F. Westrum Jr., G.C. Sinke, *The Chemical Thermodynamics of Organic Compounds*, Krieger, Malabar, FL, 1987.
- [21] M. Neurock, M. Janik, S. Wasileski, R.A. van Santen, *J. Am. Chem. Soc.*, submitted for publication (private communication).
- [22] H. Conrad, G. Ertl, E.E. Latta, *Surf. Sci.* 41 (1974) 435–446.
- [23] H. Conrad, G. Ertl, J. Koch, E.E. Latta, *Surf. Sci.* 43 (1974) 462–480; P.W. Davies, R.M. Lambert, *Surf. Sci.* 111 (1981) L671–L674; R.D. Ramsier, K.-W. Lee, J.J.T. Yates, *Surf. Sci.* 322 (1995) 243–255.
- [24] E.H. Voogt, L. Coulier, O.L.J. Gijzeman, J.W. Geus, *J. Catal.* 169 (1997) 359–364.
- [25] F. Solymosi, G. Kutsan, A. Erdohelyi, *Catal. Lett.* 11 (1991) 149–156.